

Z. LIU<sup>1,\*</sup>  
D. XI<sup>2</sup>  
D. PILE<sup>1</sup>  
Q. LUO<sup>2</sup>  
N. FANG<sup>2</sup>  
X. ZHANG<sup>1,2,✉</sup>

## Enhanced backward scattering by surface plasmons on silver film

<sup>1</sup> 5130 Etcheverry Hall, NSF Nano-scale Science and Engineering Center (NSEC), University of California, Berkeley, CA 94720-1740, USA  
<sup>2</sup> Department of Mechanical and Aerospace Engineering, University of California at Los Angeles, CA 90095-1597, USA

Received: 21 August 2006/Accepted: 15 November 2006  
Published online: 31 January 2007 • © Springer-Verlag 2007

**ABSTRACT** Surface plasmon and its potential application in nanotechnology have attracted a remarkable amount of attention recently due to their novel properties. In this work we present an angularly resolved surface plasmon scattering study on a primitive metal surface. Using a reversed attenuated total reflection (RATR) setup in the experiment, we obtained a double-crescent shaped and enhanced scattering pattern at far field. The scattering pattern as a function on the variation of angle and polarization of incident beam are studied. Both theoretical and experimental results reveal an enhanced backward scattering by surface plasmon excitation. Consequently, it is shown that this angularly resolved surface plasmon scattering measurement can be employed for resolving a richness of nanoscale surface textures.

PACS 42.79.-e; 42.30.Wb; 78.20.Ci

### 1 Introduction

Surface plasmons on metallic nano-structures offer unique opportunities for nano-scale miniaturization and integration of optical waveguides, devices and circuits [1, 2], high-resolution near-field optical microscopy [3] and lithography [4–6], surface enhanced Raman scattering allowing single-molecule detection [7, 8], etc. In particular, recent experiments demonstrated that a subwavelength superlensing effect can be achieved by surface plasmon excitation using *p*-polarized light in a silver slab [9–11].

Excitation of surface plasmons by bulk electromagnetic waves meets the difficulty that the dispersion relation of surface plasmons resides to the right of the light line. Physically this means that the incident electromagnetic waves always have insufficient momentum to excite surface plasmons for any angle of incidence. In order to couple photons into surface plasmons it is necessary to add momentum by some means. One main method is to employ a non-flat metallic surface region that can provide momentum according to available spatial frequencies provided by the surface profile. For example, periodic surface corrugations, which exhibit predominantly a single spatial frequency, provide a specific additional momentum that can be used for launching surface plasmons of

a predetermined wave number – this is often called grating coupling [12]. On the other hand defects or rough surface for example can contain a broad spectrum of spatial frequencies that can be used for exciting surface plasmons with arbitrary wavenumber [12, 13]. Another method is to increase the momentum of the incident light in a dielectric prism, consider its total internal reflection inside of the prism, and to project the evanescent field onto the metallic surface. If the component of the wavenumber in the prism parallel to the reflecting side of the prism is matched to that of surface plasmons then energy can be transferred to the surface plasmon and the reflection is no longer total – hence the name of this method attenuated total reflection (ATR) [12].

In this work, the surface plasmon scattering intensity with varying incident angle is studied using a reversed attenuated total reflection (RATR) setup. We find that the experimentally observed ratio between backward and forward scattering intensities is in good agreement with the calculation from surface scattering model using the experimentally measured surface roughness. We will show that this angularly resolved surface plasmon scattering measurement provides a means of profiling the surface nanostructure of silver film.

### 2 Theoretical background

While ATR uses a prism to couple light of a specific angle of incidence to surface plasmons, the reversed ATR (RATR) uses the opposite process and has also been used in surface plasma study [14, 15]. For RATR a metallic film is coated on one side of a high refractive index prism, surface plasmon waves on the metal/air interface are excited by roughness scattering and coupled out by prism at far side to some specific angle according to the phase matching (conservation of the tangential component of the wave vector) at the metal–prism interface. According to surface scattering theory, in the RATR configuration, the far-field light intensity  $dI$  per solid angle element  $d\Omega$  normalized by incident intensity  $I_0$  can be written as [12, 16]

$$\frac{dI}{I_0 d\Omega} = 4 \left(\frac{\pi}{\lambda}\right)^4 |T_p(k_x, d)|^2 |s(k_x)|^2 |W(\theta, \varphi)|^2, \quad (1)$$

where  $\varphi$ ,  $\theta$  and  $\lambda$  are the angle between incident plane and observation plane, the angle of observation (Fig. 2), and the incident wavelength, respectively;  $T_p$  is the *p*-polarization enhancement factor through the metallic film,  $|s(k_x)|$  is the

✉ Fax: +1-510-643-2311, E-mail: xiang@berkeley.edu

\*The first two authors contributed equally to this work

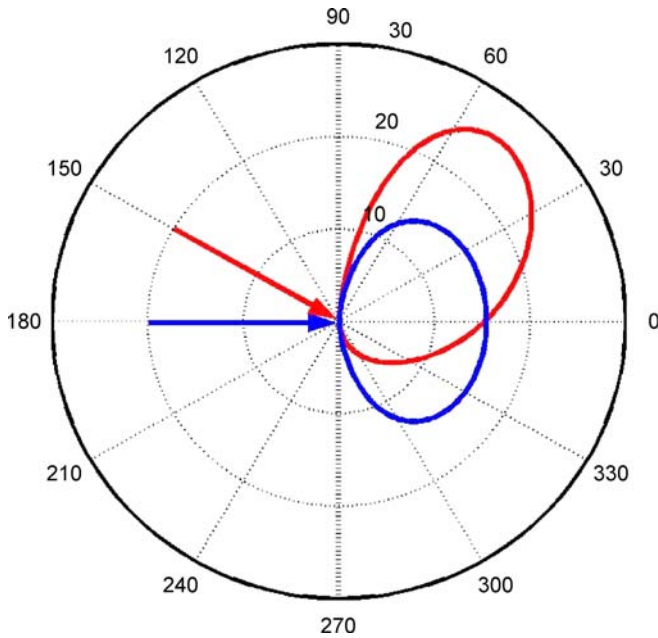


**FIGURE 1** Two example dipole functions with different incident angle given by (3). The dielectric constants used in this calculation are  $\varepsilon_1 = 1.0$ ,  $\varepsilon_2 = -9 + 0.5i$ , and  $\varepsilon_3 = 1.52$ , respectively

roughness Fourier spectrum of the metal/air interface (i.e., the Fourier amplitudes of the expansion of the surface profile  $s(x)$  into the Fourier integral), and  $W(\theta, \varphi)$  is the dipole function, which represents the angular distribution of the emitted radiation.

Enhancement factor  $T_p$  can be calculated by Fresnel equations [17]:

$$T_p(k_x, d) = \frac{t_{12}t_{23}}{\exp(-ik_{z2}d) + r_{12}r_{23} \exp(ik_{z2}d)}, \quad (2)$$

where  $r_{12} = \frac{k_{z1} - k_{z2}}{k_{z1} + k_{z2}}$ ,  $r_{23} = \frac{k_{z2} - k_{z3}}{k_{z2} + k_{z3}}$  are the reflection coefficients;  $t_{12} = 1 + r_{12}$ ,  $t_{23} = 1 + r_{23}$  are the transmission coefficients at the two interfaces; 1, 2, and 3 represent air, metal, and prism, respectively;  $k_{zj}$  represents the wave-vector at  $z$  direction within the media  $j$ .

When the observation plane is at the same plane of the incident wave (i.e.,  $\varphi = 0$ ), the angular dependent dipole function of surface scattering could be expressed as [18]:

$$W(\theta_0, \theta, \varphi = 0) = \frac{4(\varepsilon_2 - 1) \cos \theta \cos \theta_0 \left[ \times (\varepsilon_2 \sin \theta_0 \sin \theta - \sqrt{\varepsilon_2 - \varepsilon_3} \sin^2 \theta \sqrt{\varepsilon_2 - \varepsilon_1} \sin^2 \theta_0) \right]}{\left[ (\varepsilon_2 \cos \theta_0 + \sqrt{\varepsilon_2 - \varepsilon_1} \sin^2 \theta_0) \right] \left[ \times (\varepsilon_2 \cos \theta + \sqrt{\varepsilon_2 - \varepsilon_3} \sin^2 \theta) \right]}, \quad (3)$$

with  $\varepsilon_1$ ,  $\varepsilon_2$  and  $\varepsilon_3$  the dielectric constant of air, metal and prism, respectively. Figure 1, for example, shows the dipole function variation between normal incidence and angled incidence for  $p$ -polarized light. Worth mentioning is that the scattering lobe orientates backwards, a remarkable difference from dipole emission from positive dielectric interface that always points forward. This dramatic property might provide

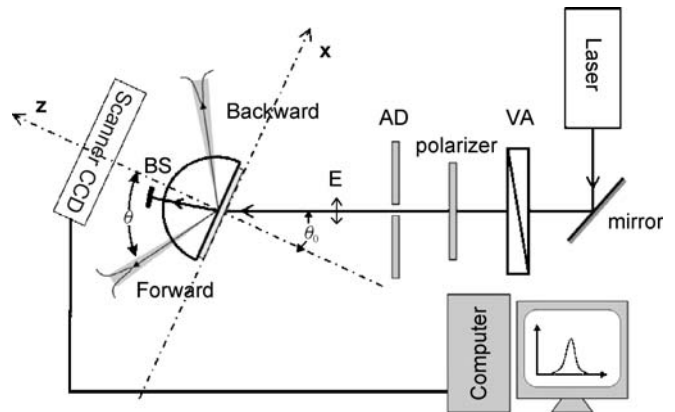
some insight to the microscopic picture of negative material properties in a metallic film for  $p$ -polarized waves. As a consequence, stronger backward scattering is expected in our experiment when the incidence is angled.

Figure 1 only represents partially the characteristics of the final scattering intensity because only those evanescent waves with  $k_x = k_{sp}$  are selectively enhanced across the metal slab and may be effectively coupled out by the prism at the very specific angle determined by  $k_{sp}$  and refractive index of prism (phase matching). It can be expected that the surface roughness spectrum also has a significant contribution to the angular distribution. In our work, the surface roughness spectrum is accurately obtained by Fourier transform of the AFM measurement of the surface profile, so that the theoretical scattering intensity distribution can be verified experimentally.

From (1), it is evident that the scattering intensity is governed by three factors: enhancement factor  $T_p$ , surface roughness spectrum  $|s(k_x)|$ , and dipole function  $W(\theta, \varphi)$ . Given any two of these three parameters, the third one can be determined by experimental measurement of  $dI/d\Omega$  and use of (1). This sets forth a surface roughness characterization method based on angularly resolved surface plasmon scattering measurement.

### 3 Experiment and discussion

The experimental setup, the angularly resolved RATR is shown in Fig. 2 schematically. A silver film, with optimized (for enhancement) 50 nm thickness, was evaporated on the flat surface of a hemispherical BK7 prism (refractive index  $n = 1.52$ ). The surface roughness was quantitatively characterized by a commercial atomic force microscope (Dimension 3100, Veeco Digital Instrument). We employed tapping mode probes (NCH-20, Nanosensors) with the acute cone angle of  $20^\circ$  and radius of curvature better than 10 nm. The obtained images of the surface profile were Fourier transformed in 2D and averaged in radial direction. The Fourier transformed surface roughness  $|S(k_x)|^2$  is plotted in Fig. 3. The two marked  $k_{sp}$  positions represent the wave numbers using to excite surface plasmons for two different wavelengths when the incident light is normal to the silver film.



**FIGURE 2** RATR setup for measuring SP scattering with varying incident angle. The direct transmission at the center of the ring is blocked by a mask. AD: aperture diaphragm (500  $\mu\text{m}$ ), VA: variable attenuator, BS: beam stopper

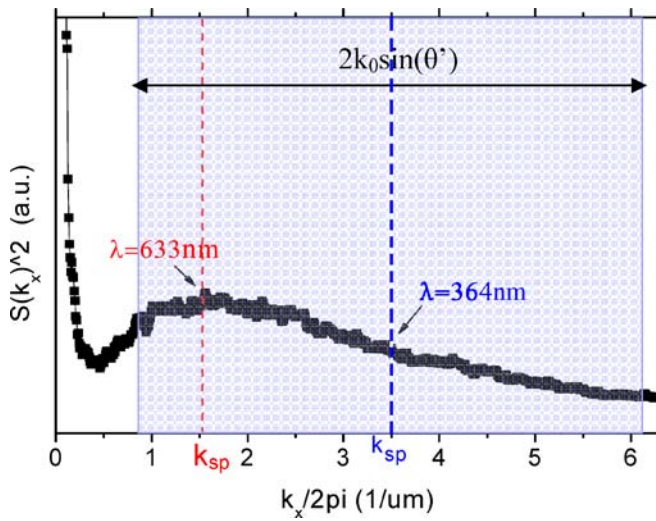


**FIGURE 3** The surface roughness spectrum by Fourier transformation of the AFM measurement.  $\theta'$  is the maximum incident angle,  $k_0$  is the  $k$  vector in free space

A collimated laser beam (polarization  $\varphi = 0^\circ$ ) with wavelength  $\lambda$  and diameter  $< 1.5$  mm was incident on the center of hemispherical prism from the flat metal-coated side. A variable attenuator was used to adjust the incident beam intensity and a polarizer was placed in front of the sample ensuring that the incident light was always  $p$ -polarized. The incident angle was controlled by a rotational stage. At the air/silver interface, a portion of the incident beam is converted from bulk waves to surface plasmons by the natural roughness coupling. These surface plasmons couple across the silver film and are allowed to be converted back to propagating waves in the hemispherical glass prism.

Behind of the sample, a computer controlled line-scan CCD was placed  $\sim 3$  cm away from the sample to detect the scattering intensity. As an example, Fig. 4a shows one of the measurement results for a non-zero angle of incidence. As can be seen, the scattering intensity in the backward (right arc) and forward (left arc) direction is very different from each other if the incident angle is not zero. Figure 4b presents the theoretical calculation result from (1) using the same non-zero angle of incidence, and we can see a good agreement with the experimental intensity distribution (Fig. 4a). The enhancement

factor, dipole function, and surface roughness spectrum used in this calculation come from (2), more general formulations than (3) including  $\varphi$  dependence [18], and Fig. 3, respectively.

Two wavelengths, 633 nm and 364 nm, were employed in our measurement. The incident angle was well defined by micro-actuated rotational stage. To further verify the simulation results, we selected the data where  $\varphi \simeq 0$  (the dashed square area in Fig. 4) and the simulated and experimental integrated intensity ratio within the selected area between backward and forward scattering will be compared. Figure 5 shows this comparison for a range of incident angles. It was found that the ratio between backward and forward scattering is around 1 for normal incidence for both the theoretical and experimental results (Fig. 5). This is expected because the dipole function is symmetrical (Fig. 1 (blue curve)) and the sample surface is isotropic. However, when the incident angle increases, the backward scattering becomes stronger than forward scattering even though the take-off angles for them are about the same (this angle only depends on the surface plasmon wave vector and the refractive index of the prism). The theoretical estimations and experimental results are consistent with each other, validating the surface scattering model we used in this study.

Consequently, this angularly resolved surface plasmon scattering measurement can be employed for the extraction of surface roughness spectrum  $|s(k_x)|$  of unknown samples. It is established that the  $k$  vector of surface spectrum ( $k_{\text{sur}}$ ) participating in surface plasmon scattering process can be written as  $k_{\text{sur}} = k_{\text{sp}} + k_0 \sin(\theta_0)$ , where

$$k_{\text{sp}} = k_0 \sqrt{\frac{\epsilon'_m \epsilon_d}{\epsilon_d + \epsilon'_m}}; \quad (4)$$

$\epsilon'_m$  represents the real part of permittivity for metal, and  $\epsilon_d$  represents the permittivity for dielectric. Therefore, for one specific incident angle, the measurement scattering intensity only relates with one specific  $k_{\text{sur}}$ . Since the enhancement factor is a constant for one fixed film thickness and fixed wavelength, the relative coefficient of the specific  $k_{\text{sur}}$  can be determined by dividing the measured intensity by the dipole function. By scanning the incident angle from  $-\theta'$  to  $\theta'$ , a broad band of spectrum information from  $k_{\text{sp}} - k_0 \sin(\theta')$  to  $k_{\text{sp}} + k_0 \sin(\theta')$  can be obtained to describe the surface morphology. Obvi-

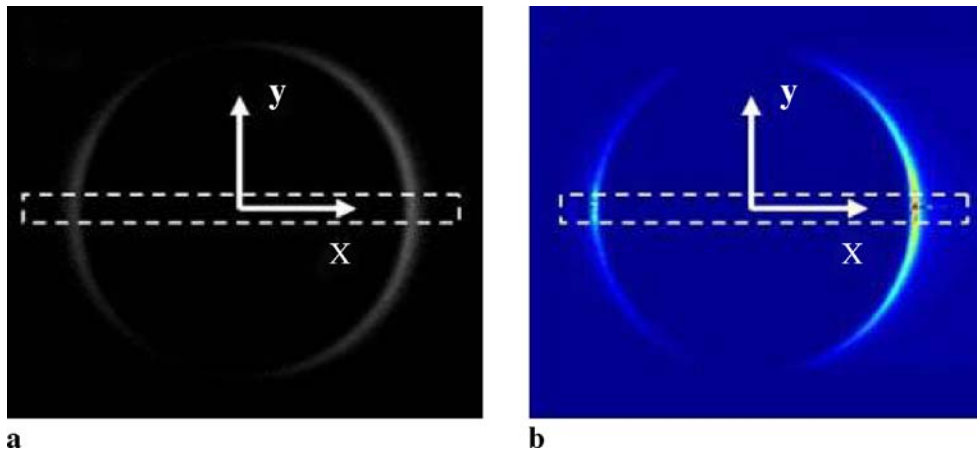


**FIGURE 4** (a) Experimentally obtained asymmetric scattering ring captured by line CCD scanner. (b) Numerically simulated intensity distribution at the same plane as for (a). Silver thickness is 50 nm, illumination light wavelength is 514 nm

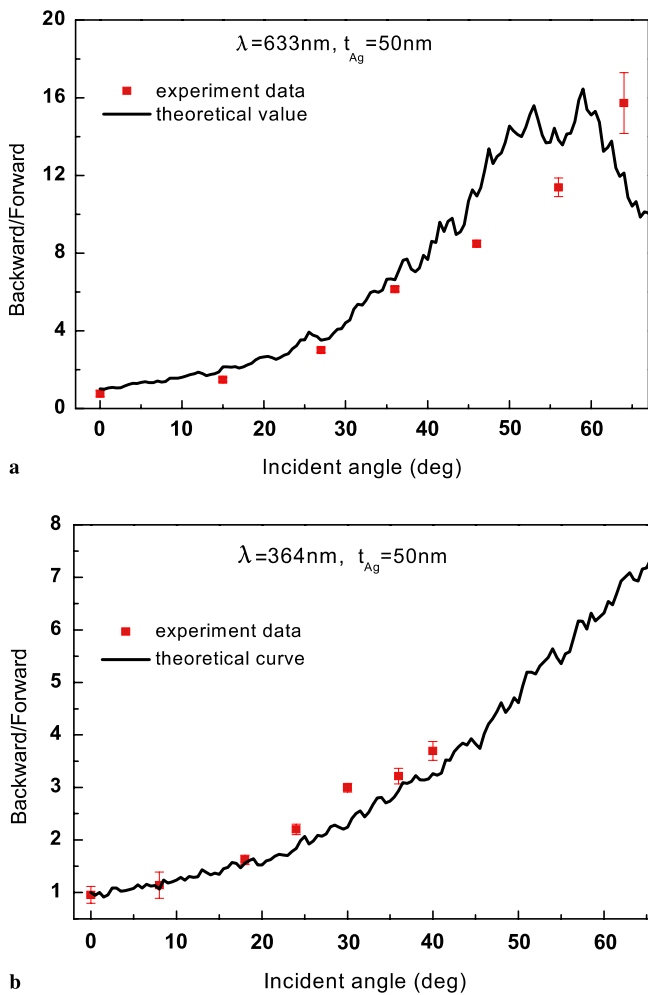


**FIGURE 5** The intensity ratio between backward scattering and for forward scattering for both measurement and calculation. (a)  $\lambda = 633 \text{ nm}$ , parameters used in calculations are:  $\epsilon_2 = -18.31 + 0.49i$  and  $\epsilon_3 = 1.5151$ . (b)  $\lambda = 364 \text{ nm}$ , parameters used in calculations are:  $\epsilon_2 = -2.54 + 0.25i$  and  $\epsilon_3 = 1.5364$

ously, a different wavelength will access a different range of surface roughness spectrum due to the difference in  $k_{sp}$ . A profile peak appears in Fig. 5a because the measurement spectrum range covers a peak surface roughness spectrum (Fig. 3); while relatively flat spectrum coverage results in a monotonous profile in Fig. 5b. If we define the morphology resolution using the highest  $k$  vector, the resolution is equal to

$$\lambda_0 / \left( \frac{k_{sp}}{k_0} + \sin(\theta') \right). \quad (5)$$

As an example, the shadowed area in Fig. 3 represents the measurable spectrum using 364nm as the probe wavelength. Assuming  $\theta' = 70^\circ$ , the resolution is around 165 nm, which is equivalent to  $\lambda/2.2$ .

From (5), it can be seen that the fundamental way to increase resolution is to increase  $k_{sp}/k_0$ . If the surrounding medium is air, this could be achieved by causing  $\epsilon'_m$  to approach  $-1$ . Notice that the  $k_{sp}$  bandwidth becomes significantly large [19], the surface spectrum can be obtained by stepping the incident angle with an in-plane wave-vector dif-

ference equal to  $k_{sp}$  bandwidth instead of a continuous scan. One of the challenges to work at this situation is that the surface plasmon wave becomes harder to be coupled out when  $k_{sp}$  goes to a higher value. As a result, grating coupler must be utilized to replace conventional optical prism.

Even though the surface roughness spectrum is easily to be extended from 1D to 2D by cooperating with a 2D rotational stage, the spectrum information only presents surface characteristics yet not an image. If we convert an image into spectrum via Fourier transform, the spectrum actually is complex. That means complete image information comprises both amplitude and phase in spectrum space, but the phase information is not able to be detected during our measurement. In order to get the surface image, a reconstruction scheme including phase retrieval algorithm might help.

#### 4 Conclusion

The angularly resolved surface plasmon scattering is studied experimentally using RATR setup. A remarkable feature is observed: due to the negative dielectric constant of the silver film, the backward scattering of the surface plasma is stronger than the forward scattering. Our measurement demonstrated that the backward-to-forward intensity ratio increases as the incident angle increases, without affecting the take-off angle. Our calculated intensity distribution surface scattering model using the experimentally measured surface roughness agrees with the experiment results very well. We further proved that up to 165 nm resolution of sub-wavelength surface textures can be resolved using 364 nm light with angularly-resolved surface plasmon scattering measurement.

**ACKNOWLEDGEMENTS** This research was partially supported by an NSF Nanoscale Science and Engineering Center (NSEC) under award number DMI-0327077 and DARPAR Negative Index Materials (NIM) program (HR 0011-05-3-0002).

#### REFERENCES

- 1 W.L. Barnes, A. Dereux, T.W. Ebbesen, *Nature* **424**, 824 (2003)
- 2 E. Ozbay, *Science* **311**, 189 (2006)
- 3 E.J. Sanchez, L. Novotny, X.S. Xie, *Phys. Rev. Lett.* **82**, 4014 (1999)
- 4 X.G. Luo, T. Ishihara, *Appl. Phys. Lett.* **84**, 4780 (2004)
- 5 W. Srituravanich, N. Fang, C. Sun, Q. Luo, X. Zhang, *Nano Lett.* **4**, 1085 (2004)
- 6 Z.W. Liu, Q.H. Wei, X. Zhang, *Nano Lett.* **5**, 957 (2005)
- 7 K. Kneipp, Y. Wang, H. Kneipp, L.T. Perelman, I. Itzkan, R.R. Dasari, M.S. Feld, *Phys. Rev. Lett.* **78**, 1667 (1997)
- 8 S.M. Nie, S.R. Emery, *Science* **275**, 1102 (1997)
- 9 N. Fang, H. Lee, C. Sun, X. Zhang, *Science* **308**, 534 (2005)
- 10 D.O.S. Melville, R.J. Blaikie, *Opt. Express* **13**, 2127 (2005)
- 11 H. Lee, Y. Xiong, N. Fang, W. Srituravanich, S. Durant, M. Ambati, C. Sun, X. Zhang, *New J. Phys.* **7**, 255 (2005)
- 12 H. Raether, *Surface Plasmons on Smooth and Rough Surfaces and on Gratings* (Springer, Berlin, 1988)
- 13 Z.W. Liu, J.M. Steel, W. Srituravanich, Y. Pikus, C. Sun, X. Zhang, *Nano Lett.* **5**, 1726 (2005)
- 14 S. Hayashi, T. Kume, T. Amano, K. Yamamoto, *Japan. J. Appl. Phys.* **35**, L331 (1996)
- 15 Z.W. Liu, N. Fang, T.-J. Yen, X. Zhang, *Appl. Phys. Lett.* **83**, 5184 (2003)
- 16 E. Kroger, E. Kretschmann, *Z. Phys.* **237**, 1 (1970)
- 17 S. Heavens, *Optical Properties of Thin Solid Films* (Dover, Mineola, 1991)
- 18 E. Kretschmann, *Opt. Commun.* **5**, 331 (1972)
- 19 N. Fang, Z.W. Liu, T.-J. Yen, X. Zhang, *Opt. Express* **11**, 682 (2003)